

Confined states in phase dynamics: The influence of boundary conditions and transient behavior

Robert J. Deissler, Y. C. Lee,* and Helmut R. Brand†

Center for Nonlinear Studies, MS-B258, Los Alamos National Laboratory, University of California, Los Alamos, New Mexico 87545

(Received 26 February 1990)

Confined states in phase dynamics—the coexistence of states with different wavelengths—are further studied. In particular, a stable and accurate numerical code is developed to study the dynamic equation of motion for two sets of boundary conditions—a pinned phase and an unpinned phase. With a pinned phase, stable confined states are found to exist for a wide range of parameter values. With an unpinned phase, the localized states are at best neutrally stable. Also, analytic solutions are found for the stationary confined states.

I. INTRODUCTION

In this paper we further study confined states in phase dynamics,^{1,2} a concept recently introduced which was motivated by experiments on Taylor-Couette flow between corotating cylinders^{3,4} and slot convection^{5,6} (Rayleigh-Bénard convection in a long, narrow, rectangular or annular container). By confined state we mean that in a stationary situation there is a dispersion in the wave number of the unit cells (rolls or vortices); i.e., a portion of the system has unit cells with wavelengths different from the wavelengths of surrounding cells. The reason for the existence of the confined state is the existence of two basins of attraction or potential wells. The system in different regions of space can therefore settle into different wells, resulting in unit cells with wavelengths different in the two regions.

The equation we study is a phase equation for a nonpropagating pattern.⁷⁻⁹ A phase equation is useful for studying the slow spatial and temporal evolution of the pattern. The physical variables A_i are of the form $A_i = A_i(k_0 x + \psi(x, t))$, where the phase ψ is a slowly varying function of space and time. Therefore, the local wave vector $q \equiv \psi_x$ will give the deviation from the background wave number k_0 . The concept of phase dynamics has not only found experimental verification slightly above onset of the instability,¹⁰ but more recently its usefulness has been experimentally demonstrated far above onset.¹¹

In Sec. II we discuss the relevant phase equation and its Liapunov functional. Much of this is a review of Refs. 1 and 2. In Sec. III we develop a highly accurate and stable code to solve the dynamic equations of motion and then study the dynamics. In Sec. IV we find analytic solutions for the stationary state. In Sec. V we conclude with comparison to and suggestions for experiment.

II. EQUATION OF MOTION AND THE LIAUPUNOV FUNCTIONAL

The phase equation we study is¹

$$\dot{\psi} = (D + E\psi_x + F\psi_x^2)\psi_{xx} - G\psi_{xxx}. \quad (1)$$

This equation has a Liapunov functional $V(\{\psi\})$ and therefore may be written as¹

$$\dot{\psi} = -\frac{\delta V}{\delta \psi}, \quad (2)$$

where

$$V(\{\psi\}) = \int_0^L dx U(\{\psi\}), \quad (3)$$

where

$$U(\{\psi\}) = \lambda\psi_x + \frac{D}{2}\psi_x^2 + \frac{E}{6}\psi_x^3 + \frac{F}{12}\psi_x^4 + \frac{G}{2}\psi_{xx}^2. \quad (4)$$

In the above, $\delta V/\delta \psi$ is the variational derivative of V with respect to ψ , i.e., $\delta V/\delta \psi \equiv \partial U/\partial \psi - \partial_x(\partial U/\partial \psi_x) + \partial_{xx}(\partial U/\partial \psi_{xx})$. Although the first term in the potential U is arbitrary as far as Eq. (1) is concerned, it is important in interpreting the results in terms of the potential for cases in which $\lambda \neq 0$ (see Sec. III). Reference 1 considered only cases where $\lambda = 0$. Such a term was previously introduced in the context of spinodal decomposition.^{12,13}

Taking the time derivative of V , we find

$$\dot{V} = - \int_0^L dx \dot{\psi}^2 + \left[\lambda + D\psi_x + \frac{E}{2}\psi_x^2 + \frac{F}{3}\psi_x^3 - G\psi_{xxx} \right] \times \dot{\psi} \Big|_0^L + G\psi_{xx}\dot{\psi}_x \Big|_0^L. \quad (5)$$

Therefore, provided the boundary terms vanish, V will be a strictly nonincreasing function of time. This guarantees global stability of ψ , assuming F and G are positive. The boundary terms will vanish for periodic boundary conditions or if

$$\lambda + D\psi_x + \frac{E}{2}\psi_x^2 + \frac{F}{3}\psi_x^3 - G\psi_{xxx} = 0, \quad (6)$$

or ψ is fixed and

$$\psi_{xx} = 0, \quad (7)$$

or ψ_x is fixed at the boundaries. Boundary conditions which will be studied in Sec. III are ψ fixed and $\psi_{xx} = 0$, and $\psi_x = \psi_{xxx} = 0$ ($\lambda = 0$).

Equation (1) may also be written in terms of the local wave vector $q \equiv \psi_x$ as

$$\dot{q} = (D + Eq + Fq^2)q_{xx} + (E + 2Fq)q_x^2 - Gq_{xxx} . \quad (8)$$

This equation may be written in terms of the Liapunov functional as

$$\dot{q} = \partial_{xx} \left[\frac{\delta V}{\delta q} \right] , \quad (9)$$

where

$$V(\{q\}) = \int_0^L dx \left[\lambda q + \frac{D}{2} q^2 + \frac{E}{6} q^3 + \frac{F}{12} q^4 + \frac{G}{2} q_x^2 \right] . \quad (10)$$

Taking the time derivative of V , we find

$$\begin{aligned} \dot{V} = & - \int_0^L dx \left[\partial_x \left[\frac{\delta V}{\delta q} \right] \right]^2 \\ & + \frac{\delta V}{\delta q} \partial_x \left[\frac{\delta V}{\delta q} \right] \Big|_0^L + Gq_x \dot{q} \Big|_0^L . \end{aligned} \quad (11)$$

This equation is equivalent to Eq. (5), as it must be.

Equation (8) for the local wave vector may be written in the form of a conservation law as²

$$\dot{q} + \partial_x j^q = 0 , \quad (12)$$

where

$$j^q = -(Dq_x + Eqq_x + Fq^2q_x - Gq_{xxx}) . \quad (13)$$

We note that the equation for the local wave vector for any phase equation $\dot{\psi} = F(\{\psi\})$ may be written as a conservation law in the form of Eq. (12), where $j^q = -F(\{q\})$ (since $q \equiv \psi_x$). It also generally follows that, if the phase is fixed at the boundaries, the q -current j^q is zero at the boundaries, and the integral of q over the system will be a constant of the motion. Fixed phase at the boundaries is the second part of condition (6) for vanishing Liapunov boundary terms. We note that for periodic boundary conditions the integral of q will also be conserved.

It also happens that Eq. (1) for the phase may be written in the form of a conservation law as²

$$\dot{\psi} + \partial_x j^\psi = 0 , \quad (14)$$

where

$$j^\psi = - \left[\lambda + D\psi_x + \frac{E}{2} \psi_x^2 + \frac{F}{3} \psi_x^3 - G\psi_{xxx} \right] . \quad (15)$$

We note that not all phase equations can be written as a conservation law for the phase. If the boundary conditions are such that the first part of condition (6) for vanishing Liapunov boundary terms is satisfied, the phase current will be zero at the boundaries and the integral of ψ over the system will be a constant of the motion.

III. NUMERICAL SOLUTION OF THE DYNAMIC EQUATION

Consider the nonlinear phase equation

$$\dot{\psi} = D(\psi_x)\psi_{xx} - G\psi_{xxx} , \quad (16)$$

where $D(\psi_x)$ is a nonlinear function of ψ_x . Equation (16) reduces to Eq. (1) for the appropriate choice of $D(\psi_x)$. The main difficulty with the numerical solution of Eq. (16) is in cases where the nonlinear diffusion coefficient $D(\psi_x)$ can become negative. Assume that $D(\psi_x)$ has a negative minimum, and let this minimum equal $-C$. We then rewrite Eq. (16) as

$$\dot{\psi} = [D(\psi_x) + C]\psi_{xx} - G\psi_{xxx} - C\psi_{xx} . \quad (17)$$

We can then use the method of time splitting¹⁴ and solve alternately

$$\dot{\psi} = [D(\psi_x) + C]\psi_{xx} \quad (18)$$

and

$$\dot{\psi} = -G\psi_{xxx} - C\psi_{xx} , \quad (19)$$

with appropriate numerical methods. Since Eq. (18) is very well behaved, we can use a second-order Crank-Nicholson method.¹⁴ Equation (19) is not very well behaved, but since it is a linear equation, we can solve it exactly using Fourier transforms. The net result is a highly accurate and stable code. We note that Eqs. (1) and (8) were not able to be successfully solved by directly using a second-order Crank-Nicholson method (with no time splitting) because of numerical instabilities.

We may also formulate the problem in terms of the local wave vector q and write

$$\dot{q} = \partial_x \{ [D(q) + C]q_x \} - Gq_{xxx} - Cq_{xx} . \quad (20)$$

Again, this equation may be split as

$$\dot{q} = \partial_x \{ [D(q) + C]q_x \} \quad (21)$$

and

$$\dot{q} = -Gq_{xxx} - Cq_{xx} , \quad (22)$$

where a second-order Crank-Nicholson method is used to solve Eq. (21) and Fourier transforms are used to solve Eq. (22).

We first solve the problem for fixed phase and $\psi_{xx} = 0$ at the boundaries [see conditions (6) and (7)]. These boundary conditions cause the integral of q to be constant. Equation (1) is scaled so that all coefficients are 1 except for E . We found it easier to implement boundary conditions for the q equation rather than the ψ equation. Therefore, we solve Eq. (20) with $D(q) = 1 + Eq + q^2$, $G = 1$, and boundary conditions $q_x = q_{xxx} = 0$ at $x = 0$ and L . Referring to Eq. (1), we see that these boundary conditions give $\dot{\psi} = 0$ and are therefore equivalent to the original boundary conditions on ψ . We alternately solve Eqs. (21) and (22) for time step Δt , except that we solve Eq. (22) for $\Delta t/2$ for the first and after the last iteration to give overall second-order accuracy. To solve Eq. (21) we use the standard second-order Crank-Nicholson method.

To solve Eq. (22) we use fast cosine transforms, since cosine satisfies the given boundary conditions. More specifically, we assume

$$q = A_0 + A_N \cos \left[\frac{N\pi x}{L} \right] + \sum_{n=1}^{N-1} 2 A_n \cos \left[\frac{n\pi x}{L} \right],$$

where

$$A_n(t + \Delta t) = A_n(t) \exp \left\{ \left[C \left(\frac{n\pi}{L} \right)^2 - G \left(\frac{n\pi}{L} \right)^4 \right] \Delta t \right\}.$$

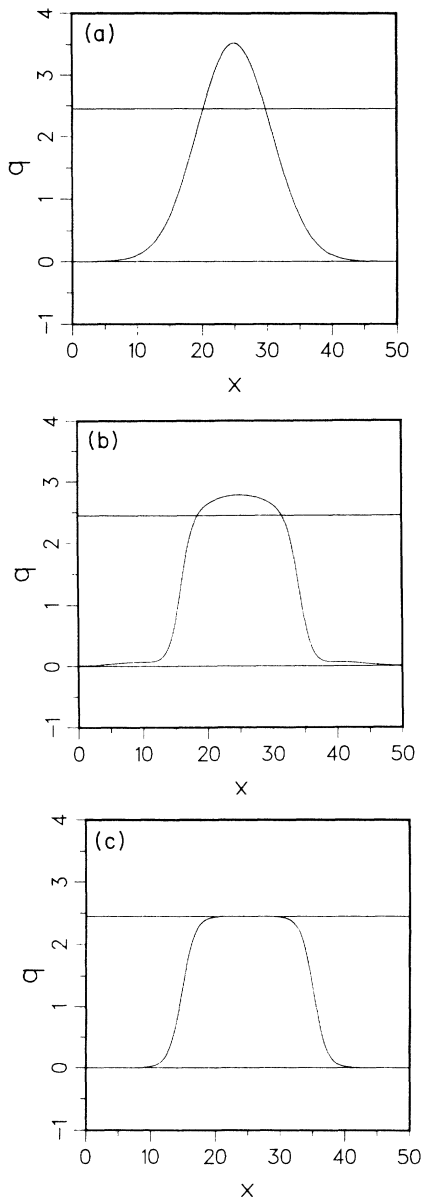


FIG. 1. Plot of the local wave vector $q \equiv \psi_x$ as a function of x at various times for $E = -\sqrt{6}$ and boundary conditions ψ fixed and $\psi_{xx} = 0$. (a) Initial Gaussian, (b) transient at $t = 10$, and (c) asymptotic state. The area under the curve $\Delta\psi \equiv \psi(L) - \psi(0) = 50$ is a constant of the motion. The asymptotic state is stable. The horizontal lines correspond to the minima of the potential seen in Fig. 2. The flat portions of q are seen to lie in the potential minima.

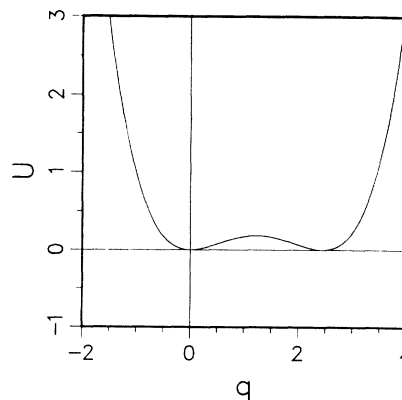


FIG. 2. Potential for the state shown in Fig. 1.

Figure 1 shows plots of q as a function of x for $E = -\sqrt{6}$ at three different times starting with an initial Gaussian [Fig. 1(a)]. We note that Eq. (1) is invariant under the transformation $E \rightarrow -E$ and $q \rightarrow -q$. Therefore, solutions for the opposite sign of E may be found by simply changing the sign of q . Since the integral of q is conserved, the area under the three curves is the same. The asymptotic state [Fig. 1(c)] is stable. In defining stability we consider only perturbations which do not change the integral of q , since the integral of q is a constant of the motion. Such perturbations will increase the Liapunov functional, and the system will return to the state which existed before the perturbation was applied. The solution in Fig. 1(c) can be thought of as a kink-antikink pair. For $q_x = 0$ the potential U from Eq. (4) is

$$U(q) = \lambda q + \frac{D}{2} q^2 + \frac{E}{6} q^3 + \frac{F}{12} q^4. \quad (23)$$

Figure 2 shows a plot of the potential $U(q)$ as a function of q for $E = -\sqrt{6}$ and $\lambda = 0$. The horizontal lines in Fig. 1 correspond to the minima of the potential. We see that the flat portions of q lie in the minima as expected. Figure 3 shows the Liapunov functional [Eq. (10)] plotted as a function of time. We see that it is strictly nonincreasing, as it must be [see Eq. (5)].

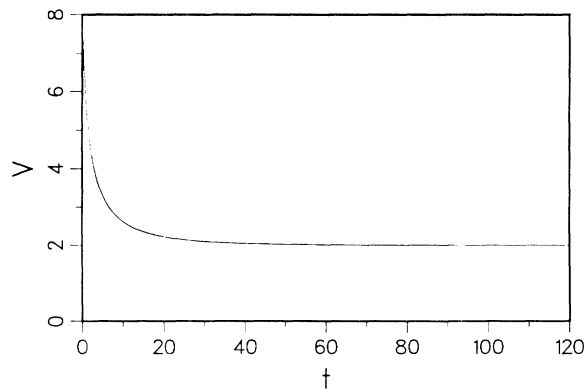


FIG. 3. Liapunov functional plotted as a function of time for the states seen in Fig. 1. It is seen to be strictly nonincreasing in time.

To see the importance of considering potentials in which $\lambda \neq 0$, we now plot in Fig. 4 the asymptotic state for other values of E , starting with the same initial condition as that in Fig. 1(a). The solid horizontal lines correspond to the minima of the potential with $\lambda = 0$. The corresponding potentials are shown in Fig. 5. We see that the flat portions of q do not lie in these minima, and in fact there is only one minimum for the third case [see Figs. 4(c) and 5(c)], although a confined state clearly exists.

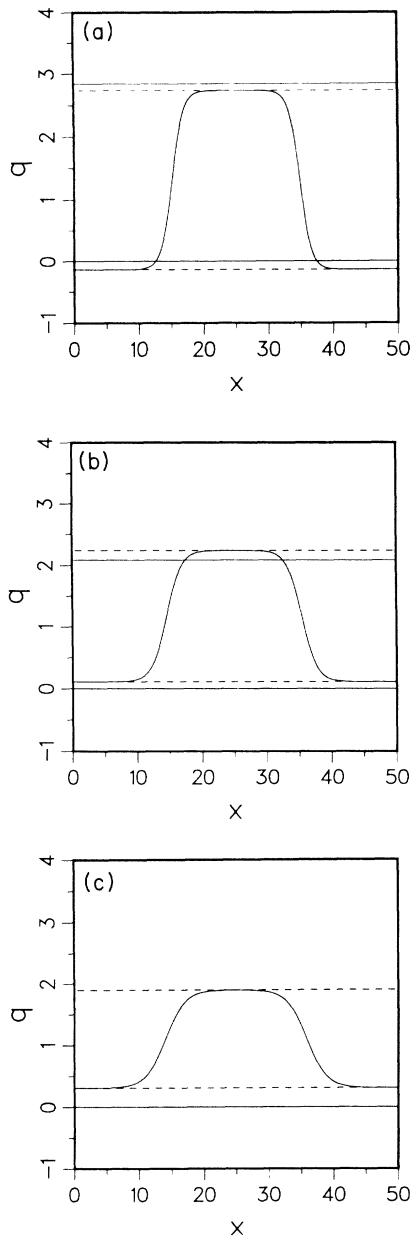


FIG. 4. Plots of the asymptotic state for various values of E starting with the same initial state and same boundary conditions as that in Fig. 1. (a) $E = -2.6$, (b) $E = -2.35$, and (c) $E = -2.2$. The solid horizontal lines correspond to the potential minima for $\lambda = 0$ (Fig. 5), and the dotted horizontal lines correspond to the potential minima for λ given by Eq. (24), (Fig. 6). The flat portions of q are seen to lie in the potential minima for the correct choices of λ .

To get the correct potential, it is necessary to consider values of λ other than zero. It turns out that the correct value of λ is determined such that the depth of the two potential wells is the same. We therefore find

$$\lambda = \frac{E}{6} \left[3 - \frac{E^2}{2} \right], \tag{24}$$

and

$$q_{\pm} = -\frac{E}{2} \pm \frac{1}{2}(3E^2 - 12)^{1/2} \text{ for } |E| > 2, \tag{25}$$

for the positions of the minima. Note that two wells exist

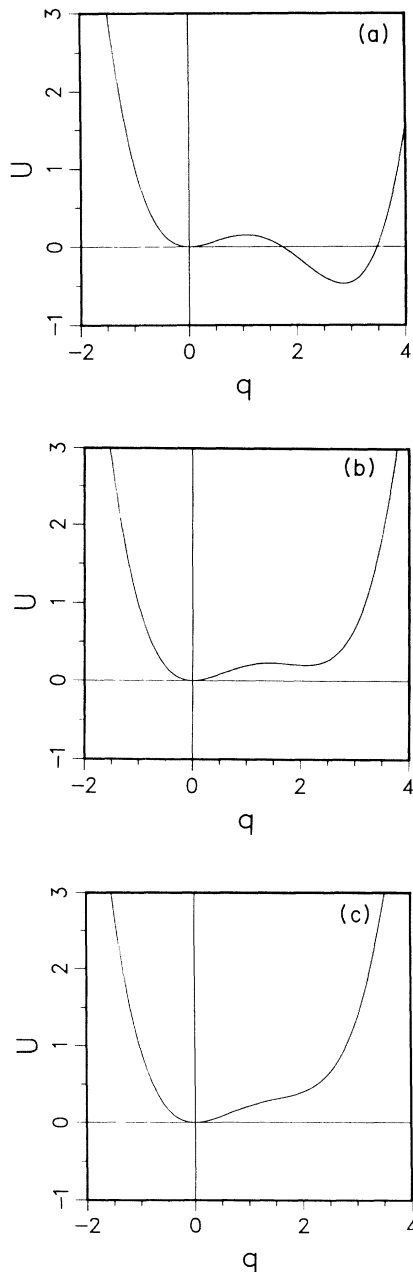


FIG. 5. Plots of the potential for $\lambda = 0$ for the states shown in Fig. 4. (a) $E = -2.6$, (b) $E = -2.35$, and (c) $E = -2.2$.

only for $|E| > 2$. Figure 6 shows plots of the potentials for these values of λ , and the horizontal dashed lines in Fig. 4 show the positions of the minima. We see that the flat portions of q now lie in these minima, as expected.

There also exist stationary solutions for cases in which the potential wells are not equal in depth. Two such solutions are shown in Figs. 7(a) and 7(b) for $E = -\sqrt{6}$. The initial conditions were again Gaussians. These solutions can be thought of as soliton and dark-soliton solutions, respectively (see Sec. IV for a qualifier on this terminology). These solutions are again stable. The horizontal

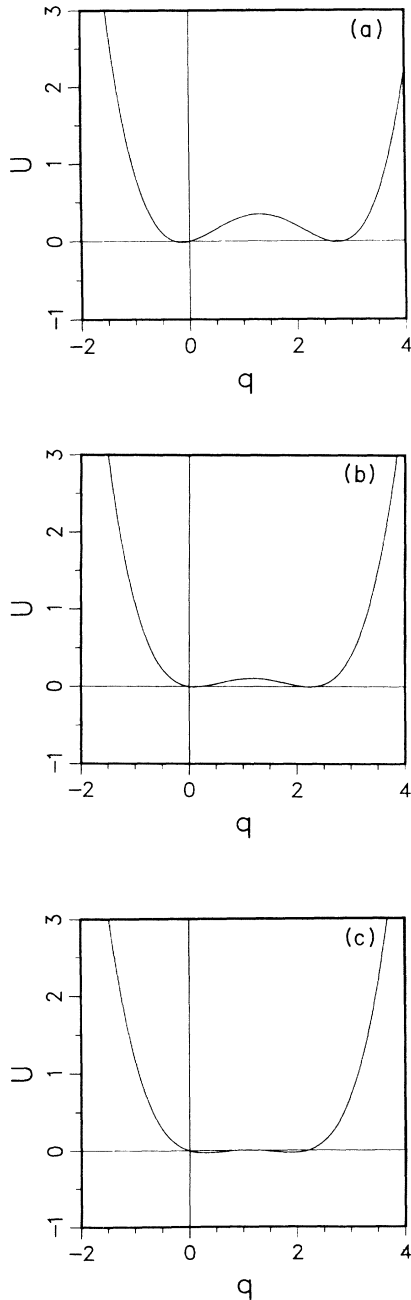


FIG. 6. Plots of the potential for λ given by Eq. (24) for the states shown in Fig. 4. (a) $E = -2.6$, (b) $E = -2.35$, and (c) $E = -2.2$.

lines correspond to the minima of the potential for $\lambda=0$ (Fig. 2). We see that the flat portions of q do not lie precisely in these minima, showing that λ is slightly different from zero. Therefore, the potential with the correct value of λ will have minima that are not equal in depth. It may be shown that the solution emerges from the shallower well (see Sec. IV).

Figure 8 shows the solution for a straight-line initial condition at different times. The asymptotic state [Fig. 8(c)] is a kink solution. Figure 9(b) shows the asymptotic solution for a two-Gaussian initial condition [Fig. 9(a)]. The stationary solutions shown in Figs. 1(c), 8(c), and 9(b) all have the same integral of q , showing that there is more than one basin of attraction for a given q integral.

To demonstrate the importance of phase pinning (for which the integral of q is conserved) in the stability of the above solutions, we now study a different set of boundary conditions, for which the phase is not pinned, namely, $\psi_x = \psi_{xxx} = 0$. These boundary conditions imply that $\lambda=0$ (since $q=0$ at the boundaries). They give vanishing Liapunov boundary terms [see Eqs. (6) and (7)], correspond to zero-phase current at the boundaries [Eq. (15)], and conserve the integral of ψ over the system. The integral of q is no longer conserved. In this case we found

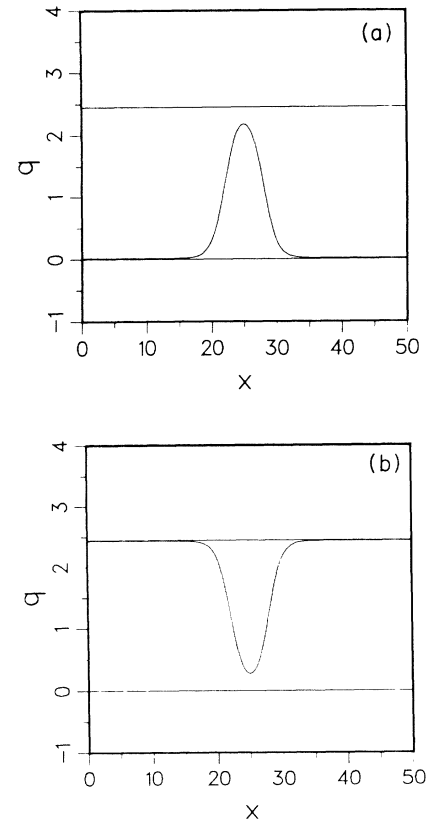


FIG. 7. Soliton and dark-soliton solutions for $E = -\sqrt{6}$ and the same boundary conditions as those used in Fig. 1. The initial conditions were a Gaussian and $\sqrt{6}$ minus a Gaussian. The area under the curve is given by $\Delta\psi$. (a) Soliton solution, $\Delta\psi = 15$; (b) dark-soliton solution, $\Delta\psi = 50\sqrt{6} - 15$. These states are stable.

it easier to solve Eq. (17) for ψ , since the boundary conditions on ψ are identical to those used previously on q . We again use the time-splitting method and solve Eqs. (18) and (19) alternately. We again use the Crank-Nicholson method to solve Eq. (18) and fast cosine transforms to solve Eq. (19).

Figure 10 shows the asymptotic state for both ψ and q for $E = -\sqrt{6}$, starting with an initial condition corresponding to that shown in Fig. 1(a), i.e., $\psi(x,0) = \int_0^x dx' q(x',0)$, where $q(x,0)$ is the Gaussian shown in Fig. 1(a). In contrast to the solution shown in

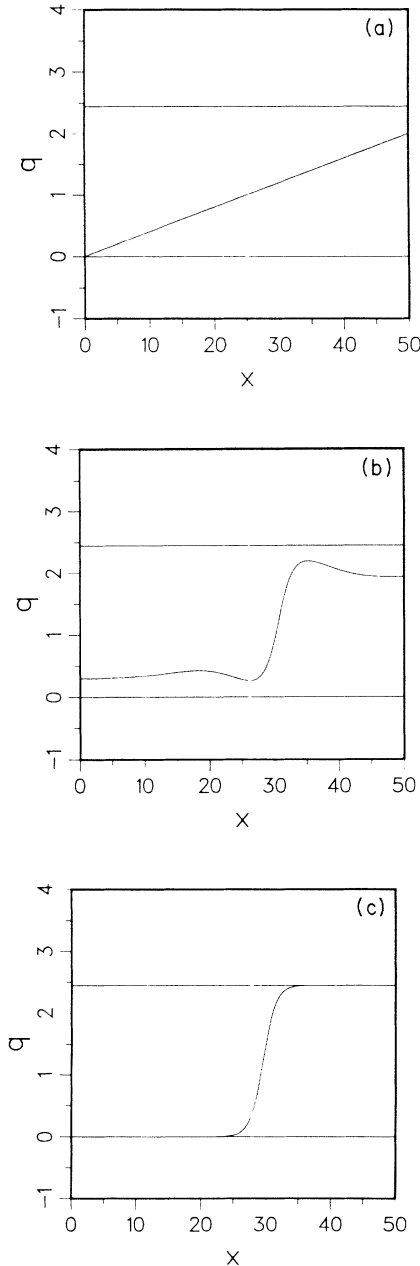


FIG. 8. Plot of q as a function of x at various times for the same value of E , same boundary conditions, and the same area $\Delta\psi$ as that in Fig. 1, but with a different initial condition. (a) Initial state; (b) transient at $t = 200$, and (c) asymptotic state.

Fig. 1(c), this solution is only neutrally stable. Since the integral of ψ is a constant of the motion, we consider only perturbations which do not change the integral of ψ . To show that the state is neutrally stable, we plot the asymptotic state for ψ for a slightly different initial condition which has the same integral of ψ . Comparing Figs. 10(a) and 11, we see that the solution in Fig. 10(a) can be perturbed to give a *new* stationary solution which has the same integral of ψ . Since the Liapunov functional is the same for these two states, the states are neutrally stable.

With these boundary conditions, neutral stability occurs only at $E = -\sqrt{6}$. To demonstrate this we now change the value of E . We first start with the state shown in Fig. 10(a) and change the parameter value to $E = -2.6$. The potential is shown in Fig. 5(a). Figure 12 shows the solution at a few different times. We see that the solution goes over to the deeper well. We again start with the state shown in Fig. 10(a), but now change the parameter value to $E = -2.35$. The potential is shown in Fig. 5(b). Figure 13 shows the solution at a few different times. We see that the solution again goes over to the deeper well. In addition, we note that soliton solutions (again, see Sec. IV for a qualifier on this terminology) are no longer stable for these boundary conditions for any

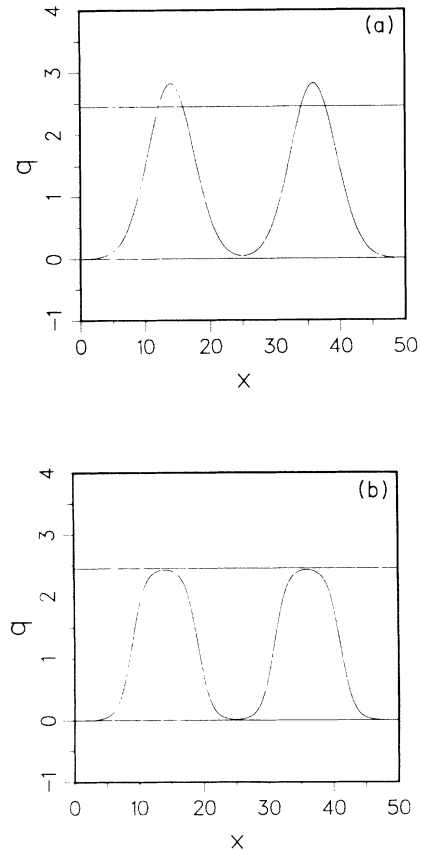


FIG. 9. Plot of q as a function of x for the initial and asymptotic states for the same value of E , same boundary conditions, and the same area $\Delta\psi$ as that in Figs. 1 and 8, but with a different initial condition. (a) Initial state (two Gaussians) and (b) asymptotic state.

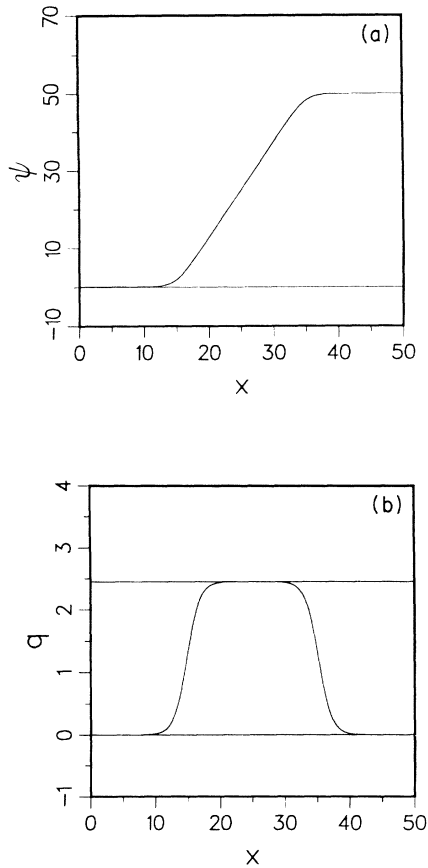


FIG. 10. Plot of the asymptotic state for both the phase ψ and $q \equiv \psi_x$ for $E = -\sqrt{6}$ starting with the same initial state as that shown in Fig. 1(a), but instead with boundary conditions $\psi_x = \psi_{xxx} = 0$. (a) ψ and (b) q . These boundary conditions do not conserve the integral of q , and the asymptotic state is neutrally stable, in contrast to Fig. 1(c) where the state is stable.

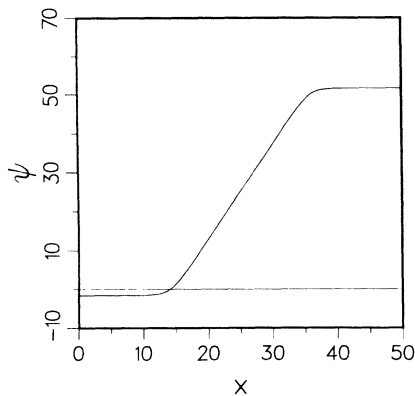


FIG. 11. Plot of the asymptotic state for the phase ψ starting with a slightly different initial condition from that used in Fig. 10. This state has the same Liapunov functional as that of Fig. 10 ($V=2$), but is clearly a different state, demonstrating neutral stability.

value of E . To see this we simply need to note that for these types of solutions the potential wells are unequal in depth. Therefore, perturbations of this solution exist which will cause the solution to go over to the deeper well.

If instead we were to impose the boundary conditions $\psi_{xx} = \psi_{xxx} = 0$, the boundaries would no longer be constrained at $q = 0$, and neutrally stable solutions would exist for a range of E , in contrast to $\psi_x = \psi_{xxx} = 0$, for which neutral stability exists only at $E = \pm\sqrt{6}$. To see this we note that if we were to start with the solution shown in Fig. 10(b) for $E = -\sqrt{6}$ and then change E to, for example, -2.6 , -2.35 , or -2.2 , the system would go over into a state such as that shown in Fig. 4(a), 4(b), or 4(c), respectively, the only difference being that the integral of q would be different from that in the figures since it is no longer conserved. The associated potential would be that shown in Fig. 6(a), 6(b), or 6(c), respectively, and the states would be neutrally stable. So we conclude this section by noting that the type of boundary conditions plays a crucial role in the existence or nonexistence of stable confined states.

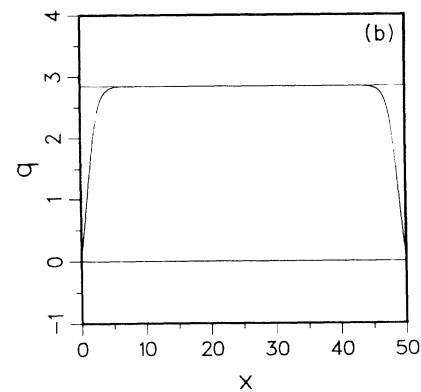
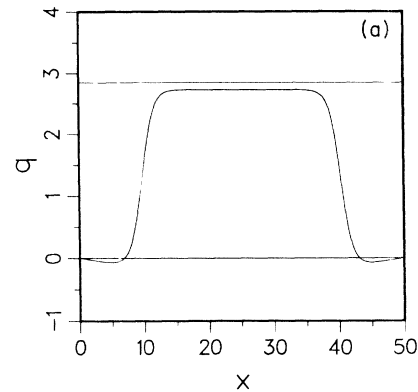


FIG. 12. Plots of q for various times with $E = -2.6$ for the boundary conditions of Fig. 10. The initial state is shown in Fig. 10(b). (a) Transient and (b) asymptotic state. The solution is seen to go over to the deeper well. See Fig. 5(a) for the corresponding potential.

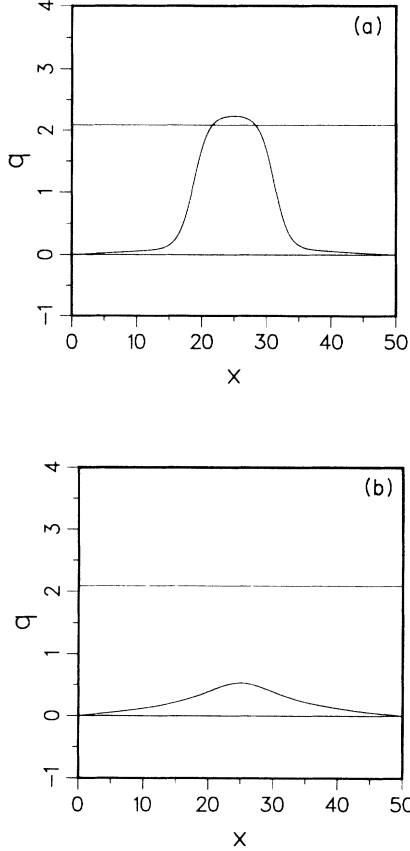


FIG. 13. Plots of q for various times with $E = -2.35$ for the boundary conditions of Fig. 10. The initial state is shown in Fig. 10(b). (a) Transient and (b) later transient. The asymptotic state is $q = 0$. The solution is seen to go over to the deeper well. See Fig. 5(b) for the corresponding potential.

IV. ANALYTIC SOLUTIONS FOR THE ASYMPTOTIC STATE

Since the Liapunov functional is strictly nonincreasing in time, the system will tend to a state in which $\delta V(\{q\}) = 0$. Taking $\delta V(\{q\}) = 0$ in Eq. (10), we therefore find

$$\lambda + Dq + \frac{E}{2}q^2 + \frac{F}{3}q^3 = Gq_{xx}, \quad (26)$$

for the ordinary differential equation satisfied by the asymptotic state. Before integrating this equation, we briefly digress by noting that Eq. (26) is useful in checking the numerical accuracy of the code used to solve the time-dependent problem. This may be done by solving Eq. (26) for λ and supplying the values for q and q_{xx} from the numerical solution. We then choose Δx and Δt small enough so that λ as given by Eq. (26) is in fact independent of x (to the desired accuracy) for the asymptotic state.

Multiplying both sides of Eq. (26) by q_x and integrating gives

$$K + U(q) = \frac{G}{2}q_x^2, \quad (27)$$

where the potential $U(q)$ is given by Eq. (23) and K is a constant of integration. From this relation one easily finds

$$\left(\frac{G}{2}\right)^{1/2} \int_{q_0}^q \frac{dq}{\sqrt{K + U(q)}} = x - x_0, \quad (28)$$

where $q_0 \equiv q(x_0)$. This is in the form of an elliptic integral. There are two special cases in which Eq. (28) reduces to elementary functions for q . When the polynomial under the square root has two double roots, a kink (or antikink) solution for q is obtained. When the polynomial under the square root has one double root, a soliton (or dark-soliton) solution is obtained. Although these solutions are not strictly solitons (or dark solitons) since Eq. (1) is nonintegrable, we nevertheless use this terminology for lack of better terms and also since solutions of this form occur in the modified Korteweg–de Vries (KdV) equation¹⁵ where they would be referred to as such.

As in Sec. III, we scale Eq. (1) so that $D = F = G = 1$ and assume that $E < 0$, noting that solutions for the opposite sign of E may be found by simply changing the sign of q . We first consider the case in which two double roots exist. We then find the following analytic expression for kink (+) and antikink (−) solutions:

$$q = \frac{q_+ + q_-}{2} \pm \frac{q_+ - q_-}{2} \tanh \left[\frac{\alpha}{2}(x - x_0) \right] \quad (29)$$

for $E < -2$,

where

$$\alpha = \left[\frac{E^2}{2} - 2 \right]^{1/2}, \quad (30)$$

and q_{\pm} and λ are given by Eqs. (25) and (24), respectively. Therefore, we find that the asymptotes correctly lie in the potential minima.

When there is a single double root, we find the following analytic expression for soliton (+) and dark-soliton (−) solutions:

$$q = q_a + \frac{2a}{-b \pm (b^2 - 4a)^{1/2} \cosh[\sqrt{a/6}(x - x_0)]}, \quad (31)$$

where

$$a = 6 + 6Eq_a + 6q_a^2,$$

$$b = 2E + 4q_a,$$

and q_a is determined from the cubic equation

$$\frac{q_a^3}{3} + \frac{Eq_a^2}{2} + q_a + \lambda = 0. \quad (32)$$

For the soliton solution, q_a equals the minimum of the three roots. For the dark-soliton solutions, q_a equals the maximum of the three roots. We note that in order to specify the limits on E for the soliton and dark-soliton solutions, it is necessary to solve the cubic equation. We only do this in the special case $\lambda = 0$ below.

When $\lambda=0$ the solutions simplify to

$$q = \frac{\sqrt{6}}{2} \left[1 \pm \tanh \left[\frac{x-x_0}{2} \right] \right] \quad \text{for } E = -\sqrt{6}, \quad (33)$$

for the kink (+) and antikink (-) solutions; to

$$q = \frac{6}{-E + (E^2 - 6)^{1/2} \cosh(x-x_0)}, \quad \text{for } E < -\sqrt{6}, \quad (34)$$

for the soliton solution; and to

$$q = q_a + \frac{2a}{-b - (b^2 - 4a)^{1/2} \cosh[\sqrt{a/6}(x-x_0)]} \quad \text{for } -\sqrt{6} < E < -4/\sqrt{3}, \quad (35)$$

where

$$q_a = -\frac{3E}{4} + \left[\frac{9E^2}{16} - 3 \right]^{1/2},$$

$$a = -12 + \frac{9E^2}{4} - 3E \left[\frac{9E^2}{16} - 3 \right]^{1/2},$$

and

$$b = -E + 4 \left[\frac{9E^2}{16} - 3 \right]^{1/2},$$

for the dark-soliton solution. Referring to the limits on E in Eqs. (33)–(35), we see that solutions exist for all values of E for which the potential [Eq. (23) with $\lambda=0$] has two minima. The kink and antikink solutions occur when the wells are equal in depth, the soliton occurs when the well at zero is shallower, and the dark-soliton solution occurs when the well at zero is deeper. Therefore, the solutions emerge from the shallower well. We note that the solutions for general λ [Eqs. (29) and (31)] can be obtained from the solutions for $\lambda=0$ [Eqs. (33)–(35)] by linear transformations in q and x . Therefore, the general solutions (29) or (31) will exist for all values of E for which the potential [Eq. (23) for general λ] has two minima: the kink and antikink solutions occurring when the wells are equal in depth, and the soliton and dark-soliton solutions occurring when the wells are unequal in depth, the appropriate solution emerging from the shallower well. Figure 12 shows the solutions (33)–(35) for various values of E . For Figs. 14(c) and 14(e), the corresponding potentials are shown in Figs. 5(a) and 5(b). We note that, as $E \rightarrow -\sqrt{6}$, the soliton and dark-soliton solutions will be well approximated by the kink-antikink and antikink-kink pairs, respectively. The Liapunov functional for the kink and antikink solutions (33) may be shown to be $V=1$. This explains why $V(t)$ in Fig. 3 approaches $V=2$ for large times, since the asymptotic state is a kink-antikink pair.

We now inquire into the stability of the analytic solutions (33)–(35) for various boundary conditions. It is assumed that the localized states are sufficiently far from boundaries so that the analytic solutions are excellent approximations to the solutions with the applied boundary

conditions. We first consider the boundary conditions ψ fixed and $\psi_{xx}=0$. As pointed out in the last section, the kink and antikink solutions (33) (or pairs of such solutions) are stable. To check for stability of the soliton and dark-soliton solutions (34) and (35), we first take the analytic states shown in Figs. 14(c) and 14(e) as initial conditions and allow the system to evolve using the numerical code discussed in the last section. We find that these equilibrium states are unstable, and the system evolves to the asymptotic states shown in Figs. 15(a) and 15(b). The reason for this behavior is that there are two equilibrium solutions (one of them unstable) for a given E and a given integral of q . Integrating Eq. (31) gives, for $\Delta\psi \equiv \psi(L) - \psi(0)$,

$$\Delta\psi = q_a L + 2\sqrt{6} \ln \left[\frac{-b \pm (b^2 - 4a)^{1/2} + \sqrt{4a}}{-b \pm (b^2 - 4a)^{1/2} - \sqrt{4a}} \right]. \quad (36)$$

Since the localized state was assumed to be far from boundaries, we extended the limits of the integral of the second term from $-\infty$ to ∞ . The + corresponds to the soliton solution and the - to the dark-soliton solution. Figures 16(a) and 16(b) show plots of $\Delta\psi$ as a function of q_a for $E = -2.6$ and -2.35 , respectively, and for $L = 50$. We indeed see that there are two solutions for a given $\Delta\psi$. The unstable solution corresponds to the intersection of the vertical and horizontal lines. Figure 17(a) and 17(b) show plots of Eq. (31) with the value of q_a given by the other intersection points of the curve with the horizontal line (found using Newton's method). We see that these plots agree with the numerical asymptotic states shown in Figs. 15(a) and 15(b). The associated potentials are shown in Figs. 18(a) and 18(b), where λ was calculated from Eq. (32). As E is increased from -2.6 (or decreased from -2.35), the two intersection points move closer together until at some E there is only a single intersection. This occurs at $E = -2.5045$ for the soliton solution and $E = -2.4035$ for the dark-soliton solution. When E is between these two values, the solution given by (34) or (35) is stable. For example, the states shown in Figs. 14(d) and 14(f) are stable. As L is increased, we find that the range of E over which the solutions (34) or (35) are stable decreases and approaches 0 as $L \rightarrow \infty$. In fact, it may be shown that the critical values of E occur at $E = -\sqrt{6}(1+1/L)$ for the soliton solution and $E = -\sqrt{6}(1-1/L)$ for the dark-soliton solution in the limit as $L \rightarrow \infty$, and therefore the range of E over which the solutions are stable approaches $2\sqrt{6}/L$. Also, the critical areas $\Delta\psi$ for the soliton solution and $q_a L - \Delta\psi$ for the dark-soliton solution approach $\sqrt{6} \ln(L)$. Since the solutions for general λ [Eqs. (29) and (31)] can be obtained from the solutions for $\lambda=0$ [Eqs. (33)–(35)] by linear transformations in q and x , we conclude in general (for these boundary conditions) that the kink and antikink solutions (or pairs of them) are stable and that the areas $\Delta\psi - q_a L$ for a soliton solution and $q_a L - \Delta\psi$ for a dark-soliton solution must be above certain values before the solutions are stable, and the critical areas increase as the length of the system increases. For very long systems we would expect only stable soliton (or dark-soliton) solutions that can be well approximated by kink-antikink (or

antikink-kink) pairs, the critical area increasing logarithmically as $L \rightarrow \infty$.

If instead we had taken the boundary conditions ψ fixed and $\psi_x = 0$, we would expect the soliton solution (34) to be stable for the full range of E indicated, since q is now fixed at the boundary and the system is no longer

free to assume a solution given by the more general Eq. (31). Likewise, with the boundary conditions ψ fixed and $\psi_x = q_a$, we would expect the dark-soliton solution (35) to be stable for the full range of E indicated. As noted in the last section, for boundary conditions $\psi_x = \psi_{xxx} = 0$, the soliton solution (34) is unstable and a kink-antikink

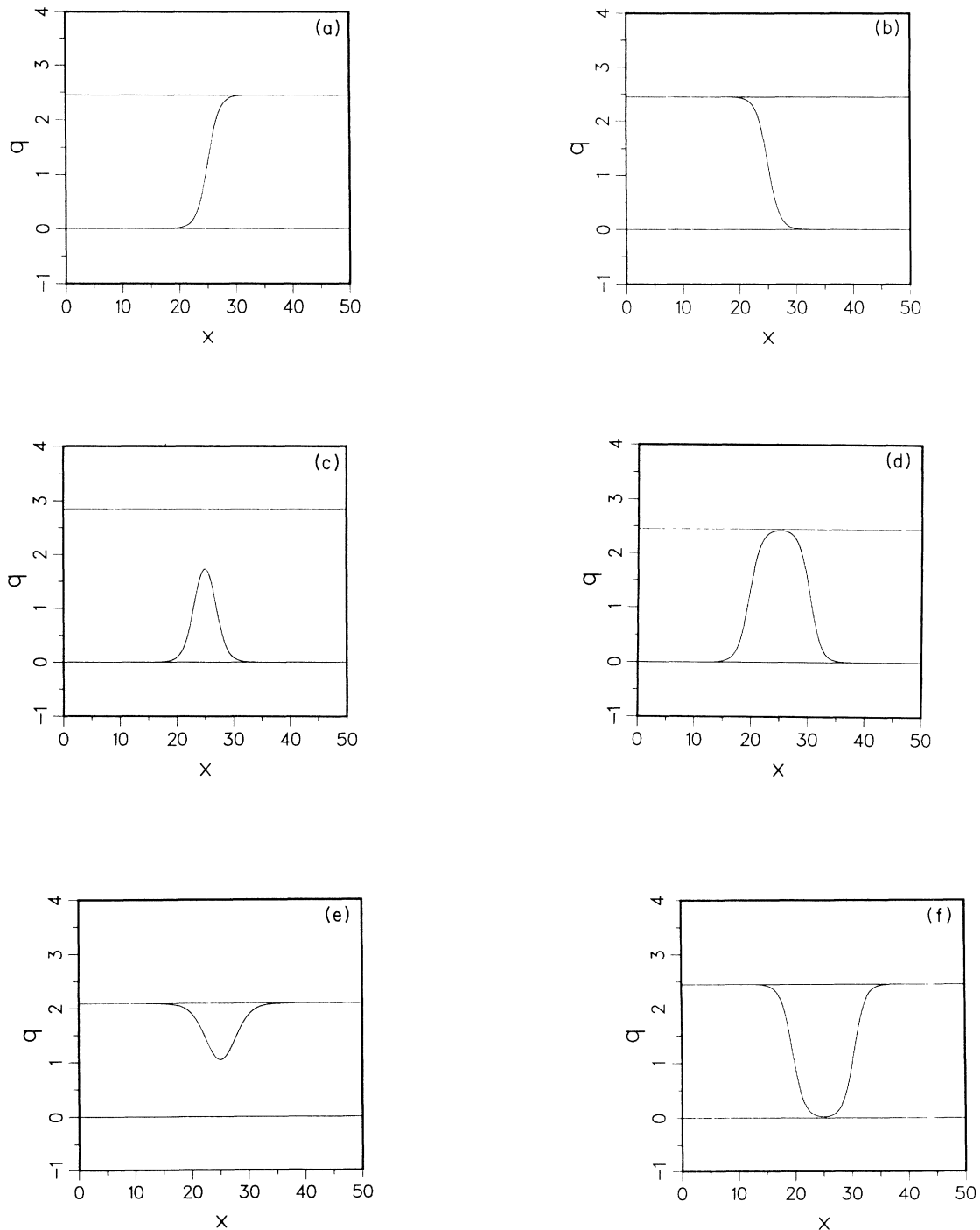


FIG. 14. Plots of analytic solutions (33)–(35). (a) Kink solution (33), $E = -\sqrt{6}$; (b) antikink solution (33), $E = -\sqrt{6}$; (c) soliton solution (34), $E = -2.6$; (d) soliton solution (34), $E = -2.4496$; (e) dark-soliton solution (35), $E = -2.35$; (f) dark-soliton solution (35), $E = -2.4494$. The corresponding potentials for (a)–(c) and (e) are plotted in Figs. 2, 2, 5(a), and 5(b), respectively.

pair (33) is neutrally stable for $E = -\sqrt{6}$. Likewise, for boundary conditions $\psi_x = q_a$ and $\psi_{xxx} = 0$, the dark-soliton solution (35) is unstable and an antikink-kink pair (33) is neutrally stable for $E = -\sqrt{6}$. For boundary conditions $\psi_{xx} = \psi_{xxx} = 0$, soliton and dark-soliton solutions (31) are unstable; and the kink and antikink solutions (29) (or pairs of them) are neutrally stable for $E < -2.2$. With these boundary conditions, the unstable soliton and dark-soliton solutions will evolve into neutrally stable kink-antikink and antikink-kink pairs, respectively.

V. EXPERIMENT AND CONCLUSIONS

Before concluding, we briefly describe the experiments which motivated the concept of confined states in phase dynamics. One experiment concerns Taylor-Couette flow^{3,4} (fluid between two concentric corotating cylinders). In this experiment a portion of the system was observed to have vortices with a wavelength larger

than that of the surrounding vortices. Although the confined state was irregular in this experiment (probably due to higher-dimensional effects), the same basic phenomenon studied in this paper and Refs. 1 and 2 is undoubtedly occurring—namely, the coexistence of two stable states along the length of the cylinders due to the existence of two wells or basins of attraction.

The second experiment concerns slot convection^{5,6} (thermal convection in a long and narrow rectangular or annular container). Since the container is narrow, the convection rolls are short and instabilities along the length of the rolls are suppressed. Therefore, this system is basically one dimensional and the confined states occurring are the same in character as those studied in this paper and in Refs. 1 and 2. In fact, the fluid equations for this system should be able to be reduced to Eq. (1). It would be interesting to try to fit the deviation from the background wave number of the rolls in the experiment to the analytic expressions given in Eqs. (29) and (31) (or their negatives).

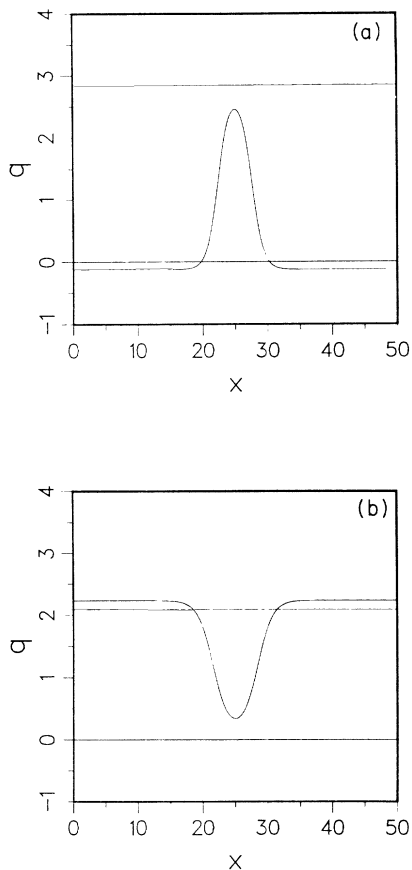


FIG. 15. Plot of the asymptotic state with the same boundary conditions as those in Fig. 1(a). The initial state is shown in Fig. 14(c); (b) the initial state is shown in Fig. 14(e). We see that the soliton and dark-soliton states shown in Figs. 14(c) and 14(e), respectively, are unstable for these boundary conditions and that the system goes to new soliton and dark-soliton state.

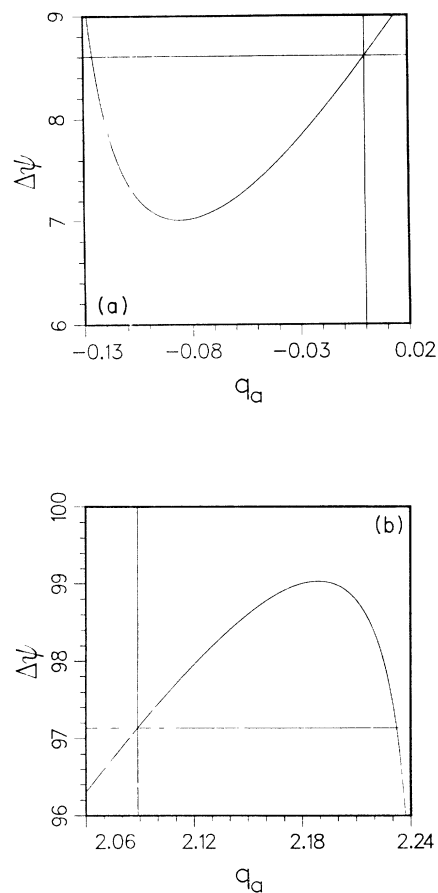


FIG. 16. Plots of $\Delta\psi$ as given by Eq. (36). (a) $E = -2.6$ and (b) $E = -2.35$. We see that there are two solutions for a given $\Delta\psi$. One intersection (with vertical line) corresponds to the unstable solutions of Figs. 14(c) and 14(e), respectively. The other intersection corresponds to the stable solutions of Figs. 15(a) and 15(b), respectively.

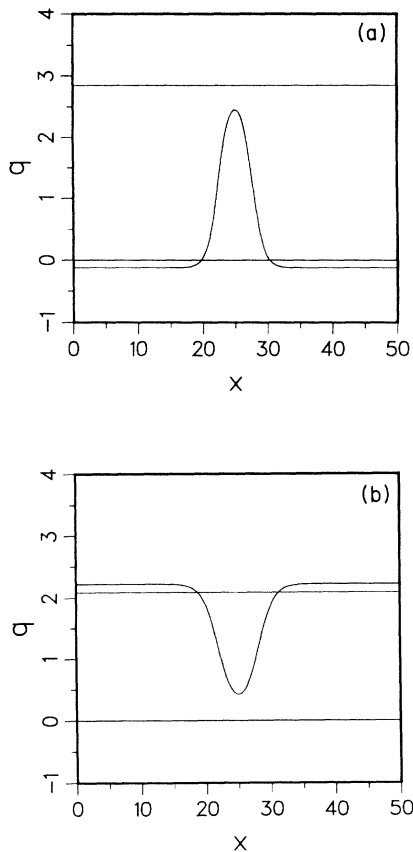


FIG. 17. Plots of the analytic solutions given by Eq. (31) with q_a given by the intersection points in Fig. 16 corresponding to the stable solutions. (a) $E = -2.6$; and (b) $E = -2.35$. We see that the analytic solutions agree with the numerical solutions shown in Figs. 15(a) and 15(b), respectively.

As found from the studies in this paper, boundary conditions play a crucial role in determining whether stable confined states exist. In the experiments mentioned above, the relevant boundary conditions are a pinned phase at the boundaries (or periodic boundary conditions for an annulus), which would explain why the states are stable. For a pinned phase or for periodic boundary conditions, the integral of q is constant and the number of rolls or vortices is conserved. As pointed out in Ref. 2, it would be interesting to change the boundary conditions by putting a ramp at the boundary, i.e., gradually change the distance between the cylinders or plates near the boundary so that the rolls gradually fade away, and are therefore not pinned and are free to move in and out of the boundary. In such a setup any localized state would at best be neutrally stable. Whether the neutrally stable states would exist only at a single value (or several distinct values) of E or over a range of E would need to be determined from experiment. In contrast, for a pinned

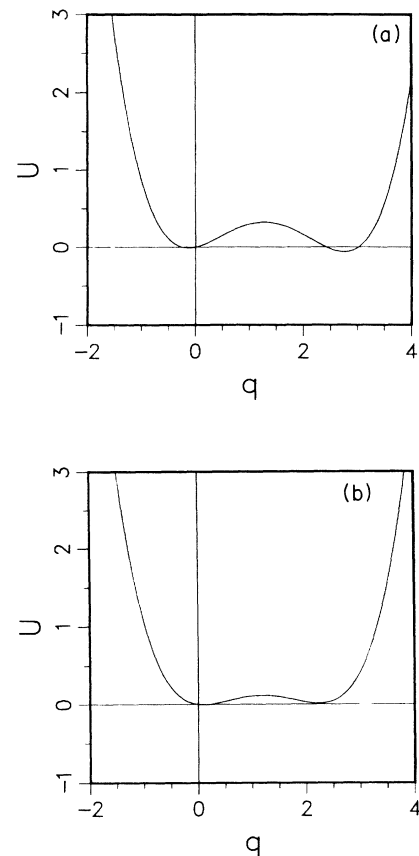


FIG. 18. Potentials corresponding to the solutions shown in Figs. 17(a) and 17(b). (a) $E = -2.6$, $\lambda = 0.14709$; (b) $E = -2.35$, $\lambda = -0.08502$.

phase, stable confined states would exist for a substantial range of parameter values.

In this paper confined states in phase dynamics were further studied. In particular, an accurate and stable numerical code was developed to solve the dynamic equation of motion for two different sets of boundary conditions—pinned phase and unpinned phase. With the pinned-phase boundary conditions, stable confined states were found to exist for a wider range of parameter values. With the unpinned phase, the localized states were at best neutrally stable. Also, analytic solutions were found for the stationary confined states.

ACKNOWLEDGMENTS

One of us (H.R.B.) thanks the Deutsche Forschungsgemeinschaft for support of his work. The work done at the Center for Nonlinear Studies, Los Alamos National Laboratory, has been performed under the auspices of the U.S. Department of Energy.

*Also at the Physics Department, University of Maryland, College Park, MD 20742.

†Also at the Fachbereich 7, Physik, Universität Essen, D-4300 Essen 1, West Germany.

¹H. R. Brand and R. J. Deissler, Phys. Rev. Lett. **63**, 508 (1989).

²H. R. Brand and R. J. Deissler, Phys. Rev. A **41**, 5478 (1990).

³G. W. Baxter and C. D. Andereck, Phys. Rev. Lett. **57**, 3046 (1986).

- ⁴C. D. Andereck and G. W. Baxter, in *Propagation in Systems far from Equilibrium*, edited by J. E. Wesfried, H. R. Brand, P. Manneville, G. Albinet, and N. Boccato (Springer-Verlag, New York, 1988), p. 315.
- ⁵M. Dubois, R. DaSilva, F. Daviaud, P. Bergé, and A. Petrov, *Europhys. Lett.* **8**, 135 (1989).
- ⁶M. Dubois (private communication).
- ⁷Y. Pomeau and P. Manneville, *J. Phys. (Paris) Lett.* **40**, L609 (1979).
- ⁸H. R. Brand, *Prog. Theor. Phys.* **71**, 1096 (1984).
- ⁹H. R. Brand, in Ref. 4, p. 206.
- ¹⁰J. E. Wesfried and V. Croquette, *Phys. Rev. Lett.* **45**, 634 (1980).
- ¹¹L. Ning, G. Ahlers, and D. S. Cannell (unpublished).
- ¹²J. S. Langer, *Ann. Phys. (N.Y.)* **65**, 53 (1971).
- ¹³J. S. Langer, *Physica* **73**, 61 (1974).
- ¹⁴W. H. Press, P. B. Flannery, S. A. Teukolsky, and W. T. Vetterling, *Numerical Recipes* (Cambridge University Press, Cambridge, England, 1986).
- ¹⁵M. Wadati, *J. Phys. Soc. Jpn.* **32**, 1681 (1972).